

# Green Synthesis of Zinc Oxide Nanoparticles Using Black Tea Extract and its Potential as Anode Material in Sodium-Ion Batteries

Hanis Mohd Yusoff<sup>1,2\*</sup>, Nurul Hayati Idris<sup>3</sup>, Nurul Fatin Hipul<sup>2</sup>, Nor Fazila Mahamad Yusoff<sup>3</sup>, Nur Zafirah Mohd. Izham<sup>2</sup> and Irshad Ul Haq Bhat<sup>2</sup>

<sup>1</sup>Advance Nano Materials (ANoMa) Research Group, Faculty of Science and Marine Environment, Universiti Malaysia Terengganu, 21030 Kuala Nerus, Terengganu, Malaysia

<sup>2</sup>Faculty of Science and Marine Environment, Universiti Malaysia Terengganu, 21030 Kuala Nerus, Terengganu, Malaysia

<sup>3</sup>Faculty of Ocean Engineering Technology and Informatics, Universiti Malaysia Terengganu, 21030 Kuala Nerus, Terengganu, Malaysia

\*Corresponding author (e-mail: hanismy@umt.edu.my)

Metal oxides have been exploited with various desired architecture due to their wide applications. One of the promising advantages of metal oxides such as zinc oxide (ZnO) is it can exhibit in many forms of nanostructures. Green synthesis approach is preferable as it is environmentally friendly and offers easy fabrication. In this study, black tea extract has been used to synthesize zinc oxide nanoparticles (ZnONPs) and further calcined at 500, 700, and 900°C. The physical properties of the ZnONPs were characterized using thermogravimetric analysis, Fourier transform infrared, scanning electron microscope, X-Ray diffraction, and Brunauer–Emmett–Teller specific surface area. The ability of the ZnONPs as anode material for sodium-ion batteries was investigated via cyclic voltammetry and galvanostatic charge-discharge. A pure phase of the ZnONPs was obtained with nanosized particles ranging from 90 to 200 nm in diameter. The ZnONPs showed a high initial discharge capacity of ~200 mAh g<sup>-1</sup> and a promising discharge capacity retention of ~60% after 100 cycles. Therefore, the ZnONP nanoparticles obtained through the green synthesis using black tea extract have a potential application as an anode in a sodium-ion battery.

**Key words:** Zinc oxide; nanoparticles; anode; sodium-ion battery

*Received: July 2019; Accepted: March 2020*

During the past years, many approaches based on the synthesis of zinc oxide nanoparticles (ZnONPs) through biological, physical as well as chemical methods have become available [1]. There are various chemical methods proposed for the synthesis of ZnONPs, such as vapour transport, the reaction of zinc with alcohol, hydrothermal synthesis, and the precipitation method [2]. However, these methods suffer from many disadvantages due to the involvement of high temperature and pressure conditions and the use of toxic chemicals [2]. Furthermore, the use of chemical methods to synthesize ZnONPs can lead to harmful by-products which are potentially risky for environmental and biological applications [2, 3]. Compared to chemical methods, the use of green synthesis methods is rapidly increasing due to the usage of less toxic chemicals, eco-friendly nature, and one-step synthesis of nanoparticles [3]. The biological systems involved in the green synthesis of nanoparticles are plants and their derivatives such as microorganisms like bacteria, fungi, algae, and yeast for synthesizing ZnONPs through biological methods with synthetic strategies. These green methods provide several advantages compared to chemical methods as they do not require really high temperature, pressure, and energy, and

most importantly no toxic chemicals that are harmful to the environment. Synthesis of ZnONPs by using plant extracts is the best alternative since it is cost effective and environmentally friendly compared to available commercial chemicals. Moreover, the physical methods used for sodium-ion battery application also do not utilize toxic chemicals and could be easily scaled up for large scale synthesis of ZnONPs. Sodium-ion batteries become an alternative to replace lithium-ion batteries since they share similar electrochemical qualities. However, sodium-ion batteries face slow ionic diffusion due to large ionic size of sodium [4, 5] and the reaction kinetics becomes sluggish. To date, only a few works have been reported for the use of ZnO as the anode for sodium-ion batteries [6-9]. The first work on ZnO as an anode in sodium-ion batteries was reported by Xu *et al.* [6]. They reported that ZnO nanowires exhibited a capacity of 650 mAh g<sup>-1</sup>. In another work [9], carbon-coated ZnO nanosheets have been synthesized via hydrothermal method. After 200 cycles, the composites exhibited a discharge capacity of ~100 mAh g<sup>-1</sup> at a current density of 100 mA g<sup>-1</sup>. In this study, we have conducted a simple and rapid green synthesis of ZnONPs by using the powder extract of black tea. Also, the ZnONPs showed a potential to

store sodium ions with an initial discharge capacity of ~200 mAh g<sup>-1</sup> at 60 mA g<sup>-1</sup>.

## EXPERIMENTAL SECTION

### Synthesis of Zinc Oxide Nanoparticles

For the preparation of the black tea extract and ZnONPs, the method was adapted and modified from Fardood *et al.* [10]. 2 g of local black tea powder (Boh tea bag) was weighed in a 50 ml beaker. The black tea powder then was added with 100 ml of distilled water. The black tea powder was boiled and maintained at 70°C for about 30 minutes until the change of colour from watery to light color of the aqueous solution. After that, the extract was cooled to room temperature. The extract was then centrifuged for 20 minutes and filtered by using the Whatman No.1 filter paper in order to be used for further experiment.

For the preparation of ZnONPs, zinc nitrate solution, zinc nitrate hexahydrate with 99% purity purchased from Sigma-Aldrich was used as the precursor in this experiment. 2 g of zinc nitrate hexahydrate was weighed and dissolved in 10 ml of distilled water. The solution was stirred constantly using a magnetic stirrer for 10 minutes.

Then, 30 ml of black tea powder extract was added and mixed homogeneously with the zinc nitrate solution in Erlenmeyer flask at 75°C. Formation of a brown precipitate occurred after continuous stirring up to 12 hours until the solution almost fully evaporated and the precipitation became a thick paste-like

solution. The precipitate was kept in an oven at 75°C overnight to dry. Samples were calcined at 500, 700, and 900°C for 4 hours in a furnace and white powders were obtained. The powders were ground to get finer particles [10].

FTIR spectra of the ZnONPs were measured to see the possible functional groups for the formation of nanoparticles. Within the range of 4000 cm<sup>-1</sup> to 400 cm<sup>-1</sup> resolution and 16 scans per sample, the FTIR analysis was recorded by using a Nicolet iS10 spectrometer. TGA measured the sample's weights whether increased or decreased upon heated or cooled condition. SEM analysis was performed to observe the morphology of the synthesized zinc oxide nanoparticles. Particle size of the ZnONPs was viewed under two different magnifications, which were 5,000X and 10,000X with an acceleration rate of 10 kV at the scale of 1 μm. The samples were scanned in all zones before images were captured. Additionally, nitrogen adsorption isotherms were obtained from accelerated surface area and porosimetry system (ASAP), and the specific surface area of the samples was obtained by using the BET method. The method involved physical adsorption of nitrogen gas at its boiling temperature. As adsorption or desorption occurred, the pressure in the sample changed until equilibrium was achieved. UV-Vis spectrophotometer is an electromagnetic radiation which includes range of ultra violet and visible light that is conducted as a wave phenomenon, characterized by a wavelength or frequency. The UV-Vis absorption spectra for the ZnO samples were recorded from 200 to 800 nm.

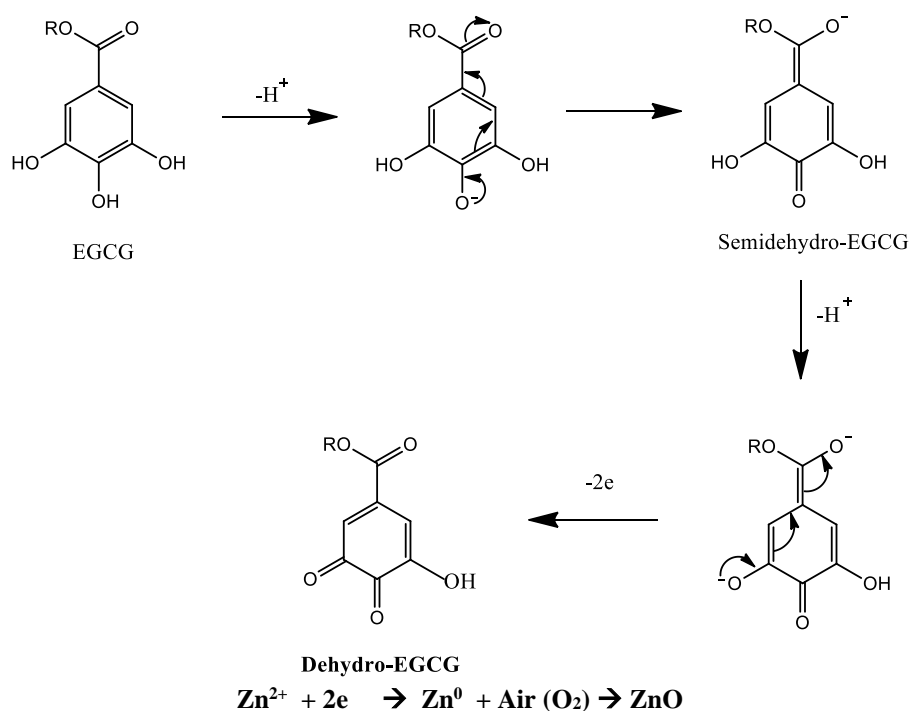


**Figure 1.** Proposed mechanism by Fardood *et al.* (2017), where epigallocatechin gallate (EGCG) is first converted into the radical ion “semidehydro-EGCG” and then into dehydro-EGCG through oxidation. Both semidehydro-EGCG and ECGC constitutes the redox system to reduce Zn<sup>2+</sup> to Zn [10].

## RESULTS AND DISCUSSION

The formation of zinc oxide nanoparticles was observed by the initial change in color, which was brown to dark brown of the aqueous solution and further confirmed with characterizations. As the aqueous solution was continuously stirred up for 12 hours, the formation of a brown precipitate was obtained. Tea is known of having water soluble

epigallocatechin gallate (EGCG) which can act as reducing and capping agents.

As shown in Figure 2, all spectra showed a broad peak between 3,000 and 4,000  $\text{cm}^{-1}$ . This was due to the vibration which indicated the functional group of O-H stretching. The presence of this band was due to adsorbed water molecules which is common in metal oxide samples [9, 10]. Wide O-H

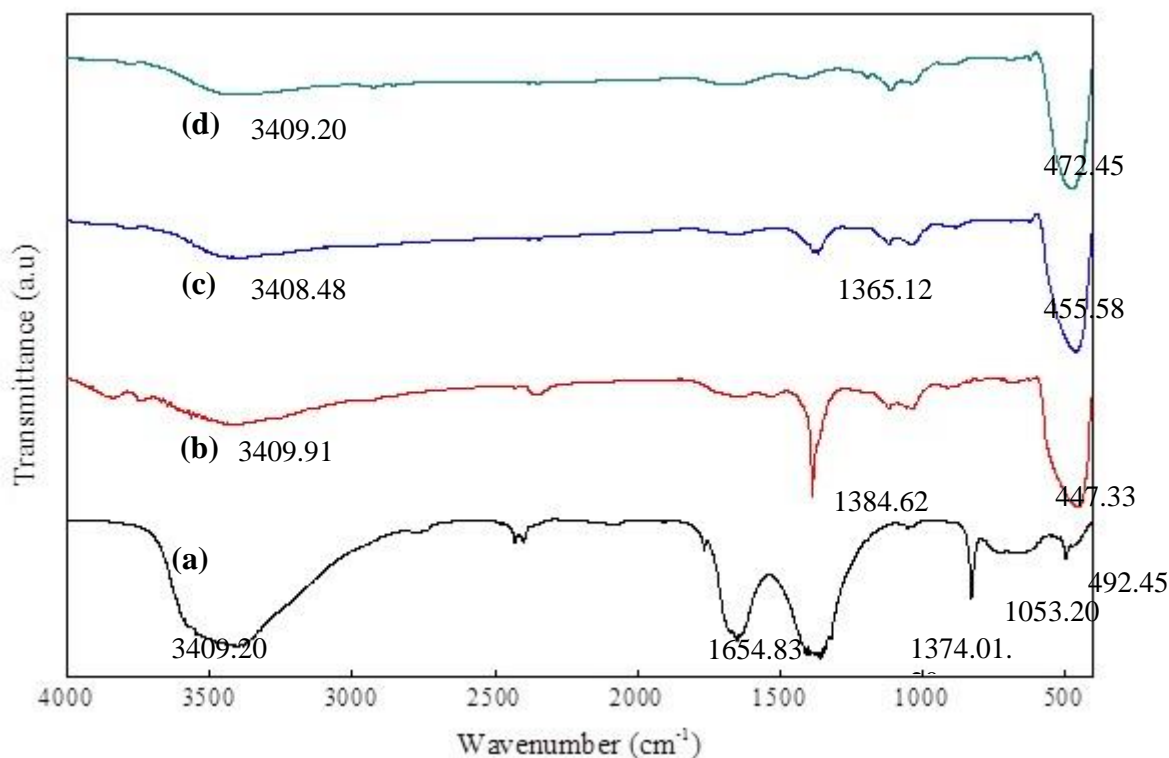


**Figure 2.** FTIR spectra of ZnO: (a) before calcined; (b) calcined at 500°C; (c) calcined at 700°C; and (d) calcined at 900°C.

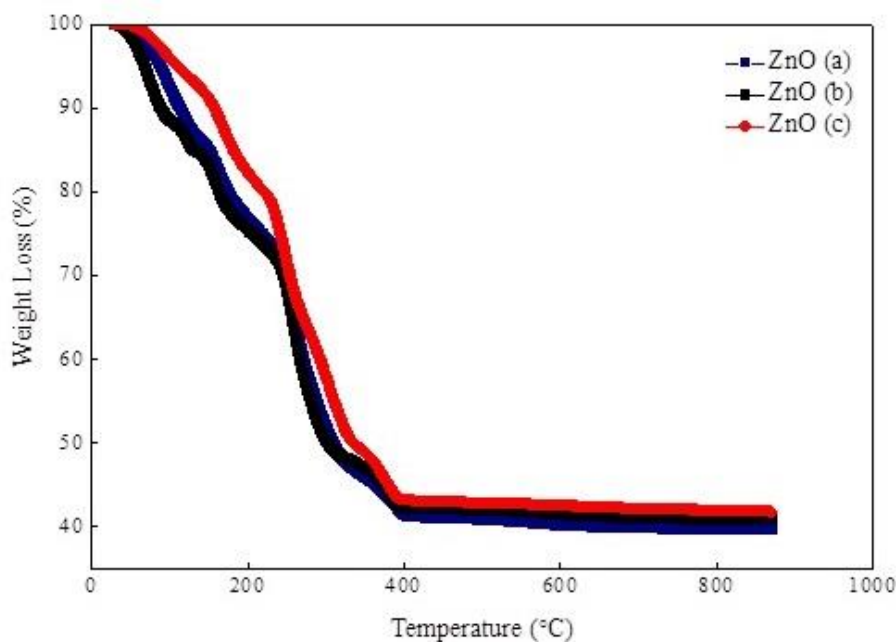


**Figure 3.** TGA graph of ZnO samples before calcinations.

peaks became narrower with increasing calcination temperature [11]. The two peaks around  $1650\text{ cm}^{-1}$  to  $1350\text{ cm}^{-1}$  may correspond to either the C-H bending or C-N stretching due to the presence of alkyl groups in tea. The mode of the vibration of C-O was observed between  $1000\text{ cm}^{-1}$  to  $1300\text{ cm}^{-1}$ . As the calcination temperature increased, precursors completely decomposed and formed ZnO, hence the disappearance of the peak at  $1654\text{ cm}^{-1}$ . There was the presence of Zn-O stretching vibration that appeared between  $447$  and  $472\text{ cm}^{-1}$ . Metal oxides generally give absorption bands in the fingerprint region below  $1,000\text{ cm}^{-1}$  arising from the inter-atomic vibrations [12]. A slight peak shift of Zn-O observed may be attributed to the change in the particle as the calcination temperatures were different [11]. Overall, the results showed that there were not many differences between the spectra except slight shifting of some of the functional groups.

Reproducibility is important in TGA analysis and 3 sets of ZnO samples using the same method were prepared separately. From Figure 2, TGA curves (b) and (c) showed the same pattern as (a), thus showed reproducibility of TGA analysis. Figure 3 shows the thermogravimetric graph of three samples of ZnO before calcination. TGA curve for the ZnO samples showed that weight loss continuously happened up to  $400^\circ\text{C}$ , and thereafter no significant

loss of heat was observed. From this information, calcination temperature chosen were  $500^\circ\text{C}$ ,  $700^\circ\text{C}$ , and  $900^\circ\text{C}$ , and it could be concluded that the formation of ZnO and complete crystallinity took place with heating at more than  $400^\circ\text{C}$  [13].

From the micrograph shown in Figure 4(a), the size of ZnONP particles calcined at  $500^\circ\text{C}$  showed a mixture of irregular shaped particles. The size for ZnO particles calcined at  $500^\circ\text{C}$  ranged from  $80\text{ nm}$  to  $430\text{ nm}$ .

From Figure 4, some mixtures of irregular shapes can be clearly be seen, which accumulated in some parts of the area. From the micrographs, it was shown that the particles have a smaller size which was in the range of  $100$  to  $200\text{ nm}$ . The size of the particles in Figure 4 seemed larger compared with ZnONPs calcined at  $500^\circ\text{C}$  and  $700^\circ\text{C}$ . An agglomeration of nanoparticles during the heating process may be due to the high surface energy of the nanoparticles [13,14]. This clearly explained that ZnONPs can obtain different particle size by varying the calcination temperature [15]. The particle sizes of ZnO were very sensitive to the calcination temperature [15]. In this study, by increasing the calcination temperature, bigger sized particles with small surface area of nanoparticles were obtained.

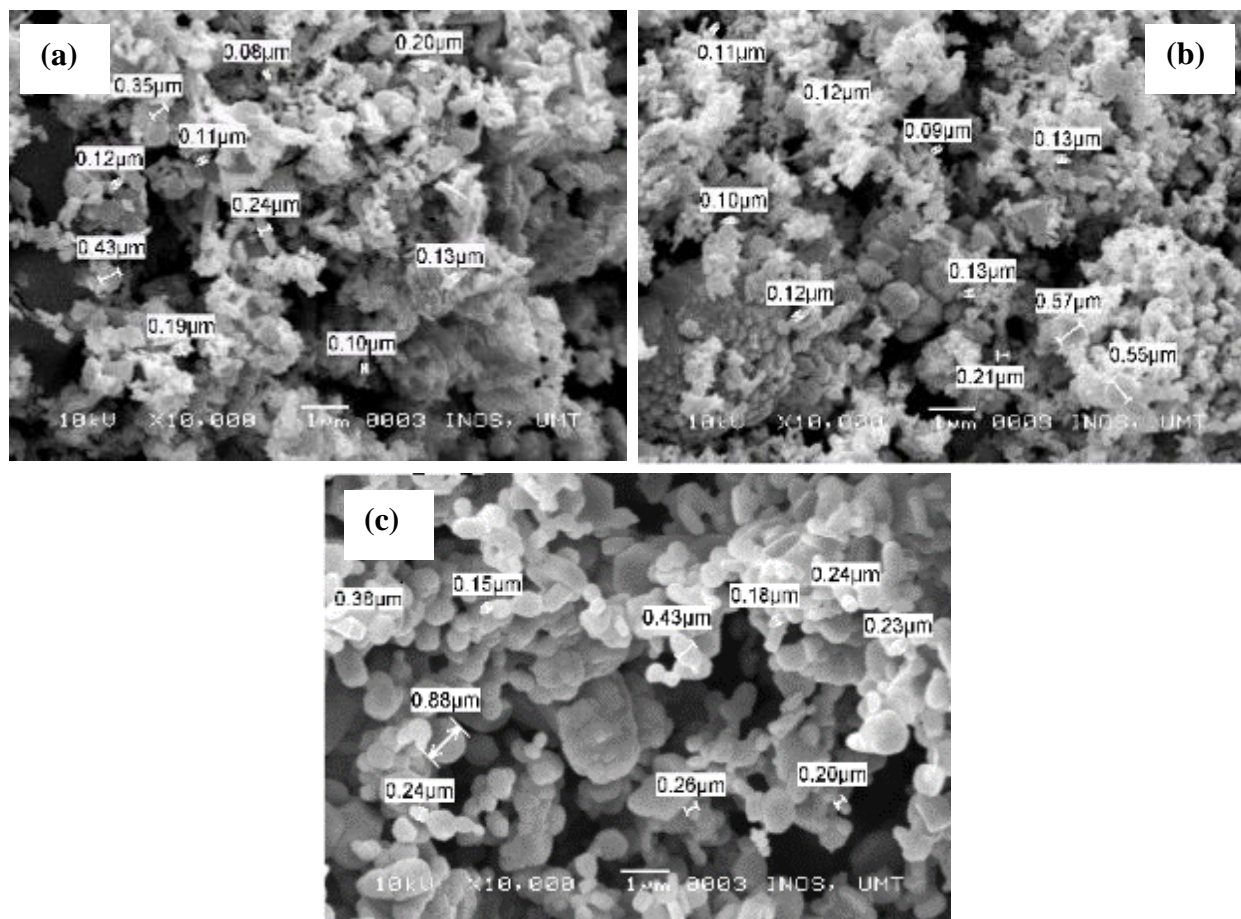


Figure 4. SEM images of ZnO calcined at: (a)  $500^\circ\text{C}$ , (b)  $700^\circ\text{C}$ , and (c)  $900^\circ\text{C}$ ; at  $10,000\times$  magnification.

Figure 5 shows the typical X-ray diffraction pattern for the samples. Based from JCPDS card No.89-1397, the ZnONPs obtained were in hexagonal wurtzite structure. All the characteristic peaks observed for the ZnONPs were in good agreement with those taken from the joint committee of powder diffraction standards (JCPDS) card No.89-1397,  $a=3.253$  nm,  $c=5.213$  nm.

The ZnONP peaks became sharper as the calcination temperature increased. Furthermore, the diffraction peak sharpness enhanced with respect to the calcination temperature and FWHM values decreased with increasing calcination temperature [16]. The three most intense peaks corresponded to the (100), (002) and (101) planes. The preferred orientation corresponded to the (101) plane which was observed for ZnONPs [11]. No peak that corresponded to the impurities were detected as it did not contain any characteristics of XRD peaks other than the ZnO peaks. This verified that pure ZnO nanoparticles were as synthesized. For average crystallite size, ZnO calcined at 500°C and 700°C shared the same value which was 28 nm. Meanwhile for ZnO calcined at 900°C, the average crystallite size deviated from this value, which was 45 nm.

For surface area study, N<sub>2</sub> absorption-desorption

measurement was carried out on isotherms of commercial ZnO and ZnO nanoparticles calcined at 500, 700 and 900°C. From the isotherms obtained, all can be classified as type IV with an apparent hysteresis loop in the low-pressure region ( $P/P^{\circ} < 0.8$ ). The adsorption and desorption isotherms were completely superpositioned, due to the adsorption of the ZnONPs samples that occurred in the micropores. In addition, in the high-pressure region ( $P/P^{\circ} > 0.7$ ), it occurred due to the capillary agglomeration and the isotherms increased rapidly and formed a lag loop [17]. For cylindrical pores, capillary condensation occurred during the adsorption via a “cylindrical meniscus”, whereas capillary evaporation occurred during desorption via a “hemispherical meniscus”. Hence, the pores of a specific size were filled at higher pressure and emptied at lower pressure, and thus the hysteresis was observed [18].

Groen *et al.* [19] suggested that the use of either adsorption and desorption branch for pore distribution calculation is often more affected by the pore network effects than the adsorption branch [20, 21]. Thus, for a purely mesoporous material, using the desorption isotherm branch is recommended for mesopore size distribution calculation. The probability pore size of commercial ZnO was estimated at about 28 nm.

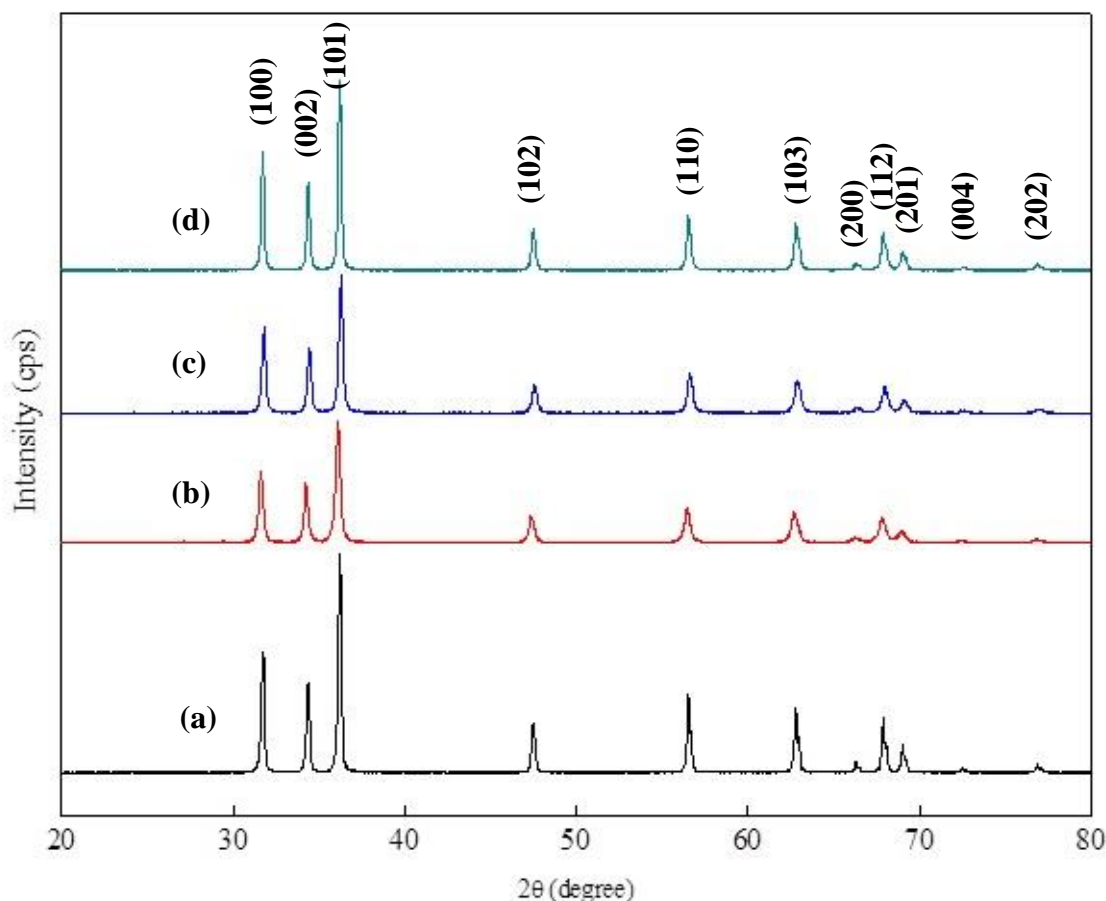


**Figure 5.** XRD diffractograms of ZnO; (a) commercial and calcined at (b) 500°C, (c) 700°C, and (d) 900 °C.

**Table 1.** BET results of commercial ZnO and ZnO calcined at 500, 700 and 900°C.

Samples	BET surface area, $S_{BET}$ (m <sup>2</sup> /g)
Commercial ZnO	4.2864
ZnO calcined 500°C	3.6011
ZnO calcined 700°C	3.9003
ZnO calcined 900°C	1.0381

All the nanoparticles had a strong absorption maximum below 400 nm, as shown in Figure 6. An obvious red shift in the absorption edge was observed for ZnO calcined at 500 and 700°C. The absorption of the nanoparticles calcined at 500 and 700°C showed wavelengths at 377 and 378 nm, respectively. According to a previous study, the absorption of UV-Vis spectrum of ZnONPs was reported between 355-380 nm [22]. One small peak observed around 700 nm in the spectrum may due to some small agglomerations of particles which were not fully

dissolved in the solution during measurement. In addition, it is known that ZnO particles which have an absorption at a higher wavelength in the UV-visible spectrum have larger particle size [23]. These data confirmed the presence of ZnONPs as the absorption bands obtained were quite similar with previous researches which deduced that the obtained peaks could be assigned to the intrinsic band gap absorption of ZnO [24]. The band gap of ZnO increased due to the increment in particle size with the increment in calcination temperature [11].

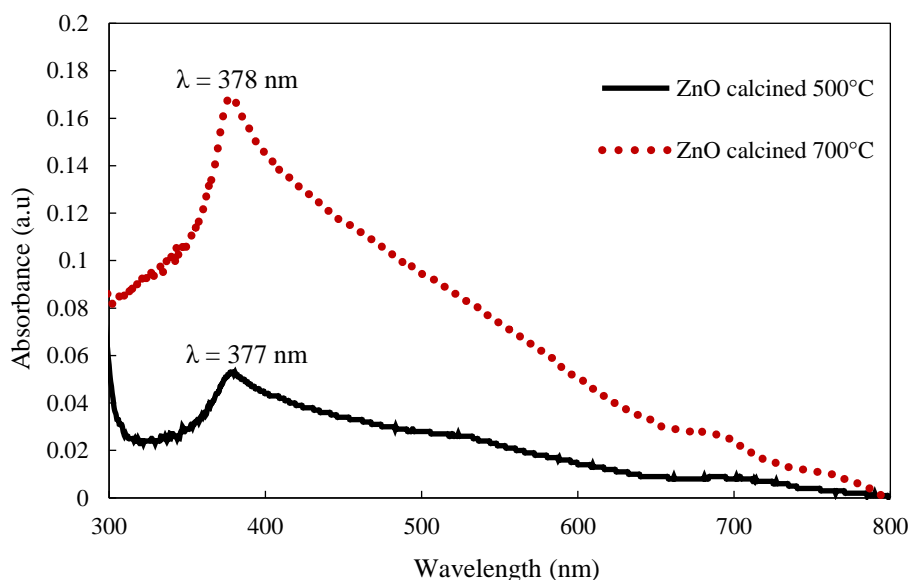


**Figure 6.** UV-Visible spectra of ZnO calcined at 500, and 700°C.

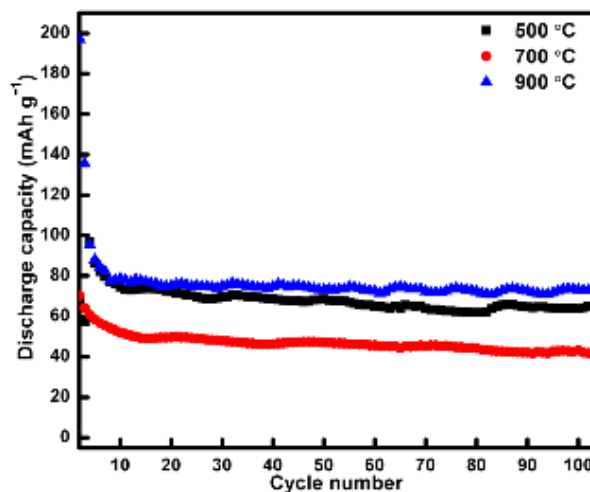
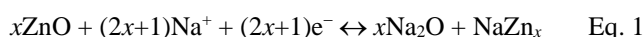


**Figure 7.** Cyclability of ZnONPs calcined at 500, 700 and 900°C over 100 cycles at a current density of 60 mA g<sup>-1</sup>.

The electrochemical stability of the ZnONPs was further confirmed by its cycling performance shown in Figure 7. The test cells were cycled at 60 mA g<sup>-1</sup> between 0.01 and 3.0 V. ZnONPs calcined at 500°C delivered an initial discharge capacity of ~90 mAh g<sup>-1</sup>, while ZnONPs calcined at 700°C delivered an initial discharge capacity of ~70 mAh g<sup>-1</sup> and exhibited a discharge capacity of ~50 mAh g<sup>-1</sup> after 100 cycles. ZnONPs calcined at 900°C displayed the highest initial discharge capacity of ~200 mAh g<sup>-1</sup> and possessed a good cycling stability over 100 cycles. After 100 cycles, the discharge capacity was ~80 mAh g<sup>-1</sup>. The galvanostatic charge/discharge curves of anode materials provided a deeper insight into the sodiation/de-sodiation process and helped to understand the reason for the poor electrochemical performance better [6].

The charge-discharge profiles at selected cycles and CV curves of ZnONPs calcined at 900°C for selected cycles are shown in Figure 8. Similar charge-discharge profiles have been reported [6, 7] and were consistent with the respective peaks in the CV curves. A clear discharge plateau at ~0.75 V related to solid electrolyte interface (SEI) formation was observed at the first cycle, and diminished upon cycling. According to Li *et al.* [6], decomposition of the electrolyte and formation of SEI on the surface of electrode particles occurred during the first cathodic cycle, which caused part of the irreversible capacity. Also, the NaZn<sub>13</sub> and Na<sub>2</sub>O phases were formed during first desodiation process, as demonstrated by Xu *et al.* [6]. The discharge profiles at 50<sup>th</sup> and 100<sup>th</sup> cycles overlapped, indicating an excellent cyclability and reversibility of the electrode. Overall, the full electrochemical reaction of the ZnONPs can be expressed as in Equation (1) [6, 25]:



The improvements on the electrochemical performance of the ZnONPs could be due to the high crystallinity, homogeneity, and uniform morphology

of the ZnONPs. At high calcination temperature, the ZnONPs became larger with low BET specific surface area, however with well established crystallinity and less agglomeration could lead to a better electric connection between the crystallites [26]. Nevertheless, for other samples, the low crystallinity and small particle size hampered their performances since large surface area could cause instability reactions between the active material and the electrolyte [27,28].

## CONCLUSION

In conclusion, this study successfully developed a biological approach to prepare ZnONPs by using black tea extract at different calcinations temperatures (500, 700 and 900°C). White ZnO powder was obtained after the calcination. The nanoparticles prepared using this method achieved uniform particle size, higher purity, well dispersed and irregular shaped. The influence of calcination temperature on the properties and morphology of the ZnONPs was investigated. The prepared samples were confirmed as ZnO through the FTIR spectra. Under the observation of SEM images, the prepared ZnO had a mixture of irregular shapes. The particle size of the ZnONPs increased as the temperature of calcination increased. The prepared samples of ZnO calcined at 500, 700 and 900°C indexed with hexagonal wurtzite structure with high crystallinity, as well as the commercial ZnO powder. A detailed study of the structure of the ZnONPs revealed a sharp peak at (101), indicating a high crystallinity. For BET surface area analysis, as the particle size of the ZnONPs increased, the surface area of the particles became smaller. The performance of each sample prepared was applied in sodium-ion batteries as a potential anode material. It was shown that the calcination temperature of ZnO at 900°C was the optimum temperature as the cyclic performance in sodium-ion battery was much better compared to ZnO calcined at 500 and 700°C. The results illustrated that the synthesized ZnO was an excellent candidate as an anode material for the sodium-ion batteries.

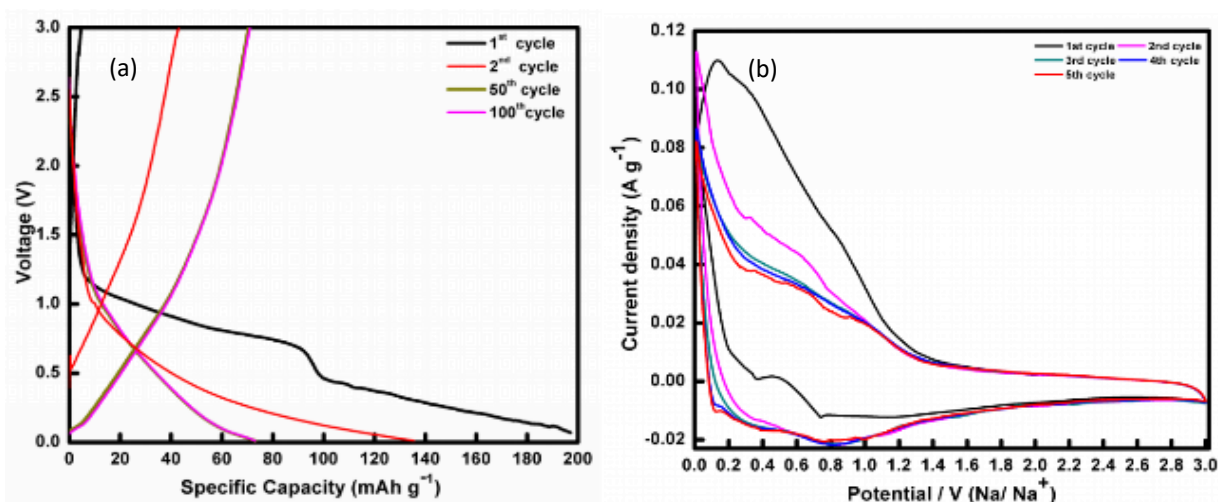


**Figure 8.** (a) Charge-discharge at selected cycles and (b) CV curves at a scan rate of 0.1 mV s<sup>-1</sup> for ZnONPs calcined at 900°C.

## ACKNOWLEDGEMENT

Authors would like to thank Universiti Malaysia Terengganu for the facilities provided and FRGS vot 59383 (FRGS/1/2015/SG01/UMT/02/3) for some fund support in this study.

## REFERENCES

1. Sutradhar, P. & Saha, M. (2016) Green synthesis of zinc oxide nanoparticles using tomato (*Lycopersicon esculentum*) extract and its photovoltaic application, *Journal of Experimental Nano-science*, **11(5)**, 314–327.
2. Sabir, S., Arshad, M., & Chaudhari, S. K. (2014) Zinc oxide nanoparticles for revolutionizing agriculture: synthesis and applications, *The Scientific World Journal*.
3. Sundrarajan, M., Ambika, S. & Bharathi, K. (2015) Plant-extract mediated synthesis of ZnO nanoparticles using *Pongamia pinnata* and their activity against pathogenic bacteria. *Advanced powder technology*, **26(5)**, 1294–1299.
4. Kim, Y., Ha, K.K., Oh, S.M. & Lee, K.T. (2014) High-capacity anode materials for sodium-ion batteries, *Chemistry—A European Journal*, **20**, 11980.
5. Yabuuchi, N., Kubota, K., Dahbi, M. & Komaba, S. (2014) Research development on sodium-ion batteries, *Chemical reviews*, **114**, 11636.
6. Xu, F., Li, Z., Wu, L., Meng, Q., Xin, H. L., Sun, J., Ge, B. L., Sun, L. T. & Zhu, Y. M. (2016) *In situ* TEM probing of crystallization form-dependent sodiation behavior in ZnO nanowires for sodium-ion batteries, *Nano Energy*, **30**, 771.
7. Teng, Y., Mo, M., Li, Y., Xue, J. & Zhao, H. (2018) Amorphous carbon-coated ZnO porous nanosheets: Facile fabrication and application in lithium- and sodium-ion batteries, *Journal of Alloys and Compounds*, **744**, 712.
8. Wan, H., Han, P., Ge, S., Li, F., Zhang, S., Li, H. (2018) Development Zinc Oxide–Cotton Fibers as Anode Materials for Lithium-Ion Batteries, *International Journal of Electrochemical Science*, **13**, 4115–4122.
9. Bresser, D., Mueller, F., Fiedler, M., Krueger, S., Kloepsch, R., Baither, D. & Passerini, S. (2013) Transition-metal-doped zinc oxide nanoparticles as a new lithium-ion anode material. *Chemistry of Materials*, **25(24)**, 4977–4985.
10. Fardood, S. T., Ramazani, A. & Joo, S. W. (2017) Sol-gel synthesis and characterization of zinc oxide nanoparticles using black tea extract, *Journal of Applied Chemical Research*, **11(4)**, 8–17.
11. Rajkumar, C. & Arulraj, A. (2018) Seed mediated synthesis of nanosized zinc oxide and its electron transporting activity in dye-sensitized solar cells. *Materials Research Express*, **5(1)**, 015029.
12. Kayani, Z. N., Saleemi, F. & Batool, I. (2015) Effect of calcination temperature on the properties of ZnO nanoparticles, *Applied Physics A*, **119(2)**, 713–720.
13. Hassan, F., Miran, M. S., Simol, H. A., Susan, M. A. B. H. & Mollah, M. Y. A. (2015) Synthesis of ZnO nanoparticles by a hybrid electrochemical-thermal method: influence of calcination temperature, *Bangladesh Journal of Scientific and Industrial Research*, **50(1)**, 21–28.
14. Kumar, H. & Rani, R. (2013) Structural and optical characterization of ZnO nanoparticles synthesized by microemulsion route, *International Letters of Chemistry, Physics and Astronomy*, **14**, 26–36.
15. Hong, R. Y., Qian, J. Z. & Cao, J. X. (2006) Synthesis and characterization of PMMA grafted ZnO nanoparticles, *Powder Technology*, **163(3)**, 160–168.
16. Thirumavalavan, M., Huang, K. L. & Lee, J. F. (2013) Preparation and morphology studies of nano zinc oxide obtained using native and modified chitosans, *Materials*, **6(9)**, 4198–4212.
17. Wang, Y., Zhang, C., Bi, S. & Luo, G. (2010) Preparation of ZnO nanoparticles using the direct precipitation method in a membrane dispersion micro-structured reactor, *Powder Technology*, **202(1-3)**, 130–136.
18. Salahuddin, N. A., El-Kemary, M., Ibrahim, E. M. (2015) Synthesis and characterization of ZnO nanoparticles via precipitation method: Effect of annealing temperature on particle size, *Nanoscience and Nanotechnology*, **5(4)**, 82–88.
19. Zhou, M., Wei, Z., Qiao, H., Zhu, L., Yang, H., & Xia, T. (2009) Particle size and pore structure characterization of silver nanoparticles prepared by confined arc plasma, *Journal of Nanomaterials*, **3**.
20. Gregg, S. J., Sing, K. S. W. (1982) Adsorption surface area and porosity, second ed., *Academic Press, London*, **303**
21. Groen, J. C., Peffer, L. A. & Pérez-Ramírez, J. (2003) Pore size determination in modified micro-and mesoporous materials. Pitfalls and limitations in gas adsorption data analysis,

- Microporous and mesoporous materials*, **60(1-3)**, 1–17.
22. Everett, D. H. & Haynes, J. M. (1972). Model studies of capillary condensation: I. Cylindrical pore model with zero contact angle, *Journal Colloid and Interface Science*, **38(1)**, 125–137.
  23. Liu, H., Zhang, L. & Seaton, N. A. (1993) Analysis of sorption hysteresis in mesoporous solids using a pore network model, *Chemical Engineering Science*, **156(2)**, 285–293.
  24. Juan, E. U., Alejandro C. A., Martha S. G., Abraham, M. A. & Alma V. D. (2018) Nanoscale zinc oxide particles for improving the physiological and sanitary quality of a Mexican landrace of red maize, *Nanomaterials*, **8(4)**, 247.
  25. Stan, M. C., Klopsch, R., Bhaskar, A., Li, J., Passerini, S. & Winter, M. (2013) Cu<sub>3</sub>P binary phosphide: synthesis via a wet mechanochemical method and electrochemical behavior as negative electrode material for lithium-ion batteries, *Advanced Energy Materials*, **3**, 231–238.
  26. Chieng, B. W. & Loo, Y. Y. (2012) Synthesis of ZnO nanoparticles by modified polyol method, *Materials Letters*, **73**, 78–82.
  27. Rosedhi, N. D. & Idris, N. H. (2019) Electrochemical performance of LiNi<sub>0.5</sub>Mn<sub>1.5</sub>O<sub>4</sub> synthesised via ball-milling for Li-ion batteries, *Ionics*, **25**, 2069–2076.
  28. Mokhtar, N., Idris, N. H. & M. F. Md Din, M. F. (2018) Molten Salt Synthesis of Disordered Spinel LiNi<sub>0.5</sub>Mn<sub>1.5</sub>O<sub>4</sub> with Improved Electrochemical Performance for Li-ion Batteries, *International Journal of Electrochemical Science*, **13**, 10113–10126